Dalton Transactions

ROYAL SOCIETY OF CHEMISTRY

PAPER

View Article Online
View Journal | View Issue

Cite this: *Dalton Trans.*, 2024, **53**, 16397

Catalytic evaluation of MOF-808 with metallic centers of Zr(IV), Hf(IV) and Ce(IV) in the acetalization of benzaldehyde with methanol†

Yazmín Arellano,[a,b] César Pazo,[a,b] Vanesa Roa,[a,b] Yoan Hidalgo-Rosa,[c,h] Ximena Zarate,[d] Jaime Llanos,[e] Nestor Escalona[b,f,g] and Eduardo Schott *[a,b]

In the context of climate change, it is of utmost importance to replace the use of fossil fuels as raw material in areas of industrial interest, for example, in the production of chemical inputs. In this context, a viable option is biomass, since by subjecting it to chemical processes such as pyrolysis, it is possible to obtain platform molecules that are the basis for the generation of value-added chemical products. Acetals are molecules obtained from biomass derivatives, which have various applications in cosmetic chemistry, in the pharmaceutical industry as intermediates or final compounds, food additives, among others. Different catalysts have been used in the acetalization reaction, including MOFs, which have the advantage of being porous materials with high surface area values. The large surface area translates into a greater number of catalytically active sites available for the reaction. Among the MOFs that have been used for this purpose is MOF-808, which is characterized by having a lower number of ligands attached to its metal cluster, therefore, it has a greater exposure of the metals that make up its structure. In this context, the work carried out studied the catalytic performance of MOF-808 when its Zr(IV) metal centers are replaced by Hf(IV) and Ce(IV) atoms in the acetalization reaction of benzaldehyde with methanol. The MOFs obtained by solvothermal synthesis were characterized by powder X-ray diffraction, N_2 adsorption and desorption, FT-IR spectroscopy, acid–base potentiometric titration, XPS and thermogravimetric analysis. The results of the catalysis indicate that the MOF with the best performance was MOF-808-Ce, which achieved conversions greater than 80% in a period of ten minutes. MOF-808-Ce exhibits a higher number of defects and therefore a higher availability of catalytic sites for the reaction to occur, which explains the better performance. Finally, the performance of MOF-808 in the acetalization of benzaldehyde with methanol was also supported by density functional theory (DFT) calculations.

Received 7th July 2024,
Accepted 9th September 2024

DOI: 10.1039/d4dt01959h

rsc.li/dalton

[a]*Departamento de Química Inorgánica, Facultad de Química y de Farmacia, Centro de Energía UC, CIEN-UC, Pontificia Universidad Católica de Chile, Avenida Vicuña Mackenna, 4860, Santiago, Chile. E-mail: maschotte@gmail.com*
[b]*ANID-Millennium Science Initiative Program-Millennium Nuclei on Catalytic Process Towards Sustainable Chemistry (CSC), Chile*
[c]*Centro de Nanotecnología Aplicada, Facultad de Ciencias, Ingeniería y Tecnología, Universidad Mayor, Camino La Pirámide 5750, Huechuraba, Santiago, Chile 8580745*
[d]*Instituto de Ciencias Aplicadas, Facultad de Ingeniería, Universidad Autónoma de Chile, Santiago, Chile*
[e]*Departamento de Química, Facultad de Ciencias, Universidad Católica del Norte, Antofagasta, Chile*
[f]*Departamento de Ingeniería Química y Bioprocesos, Escuela de Ingeniería, Pontificia Universidad Católica de Chile, Avenida Vicuña Mackenna 4860, Macul, Santiago, Chile*
[g]*Departamento de Química Física, Facultad de Química y de Farmacia, Pontificia Universidad Católica de Chile, Vicuña Mackenna 4860, Santiago, Chile*
[h]*Escuela de Ingeniería del Medio Ambiente y Sustentabilidad, Facultad de Ciencias, Ingeniería y Tecnología, Universidad Mayor, Camino La Pirámide 5750, Huechuraba, 8580745 Santiago, Chile*

† Electronic supplementary information (ESI) available. See DOI: https://doi.org/10.1039/d4dt01959h

Introduction

The current climate crisis, associated with the increase in the emission of greenhouse gases generated by the excessive use of fossil fuels, makes it an urgent necessity to replace oil as a raw material in different industrial sectors,[1–3] for example in the fabrication of chemical products where an option that appears in the last decades is the use of lignocellulosic biomass as a raw material.[1,4–7] This type of biomass is the only carbon renewable source worldwide[8] and consists of the organic material produced by plants through photosynthesis.[9] The composition of lignocellulosic biomass, specifically its high content of aromatic compounds, allows its use as a source of platform molecules relevant to the chemical industry[6,10,11] such as aldehydes that can be transformed into acetals. Acetals have applications in cosmetic chemistry, in the pharmaceutical industry as intermediates or final compounds, food additives, among others.[12–14] These molecules are usually

prepared by the acetalization reaction in the presence of a catalyst with acid sites in its structure.[12–14] A representative case of this reaction is the benzaldehyde acetalization with methanol producing (dimethoxymethyl)benzene. Different catalysts have been used in this reaction (either homogeneous[16,17] or heterogeneous[18–20] catalysts). An example of heterogeneous catalysts used in this reaction are Metal Organic Frameworks (MOFs). MOFs are a subfamily of coordination polymers, have been lately studied as heterogeneous catalysts. MOFs are formed by metallic clusters, denominated secondary building units (SBUs), bonded to organic ligands through coordination bonds generating three-dimensional porous structures[15,16] characterized by their high porosity, surface areas, and crystallinity.[17,18] Another important characteristic of MOFs is their large structural diversity due to the different ligands and metallic centers that can be used. This has allowed these materials to be used in different applications such as gas storage, chemical separation, sensing, drug delivery, catalysis, and others.[19–21] HKUST-1,[22,23] UiO-66,[24–26] UiO-67,[26] and MOF-808 are MOFs that have been widely applied as catalysts in the methanol benzaldehyde acetalization reaction because all these materials have acid catalytic active sites in their structure.[27] Dhakshinamoorthy and collaborators,[28] reported their work with HKUST-1 (which is constituted by copper metal centers), and evaluated the use of different alcohols in the acetalization reaction of benzaldehyde. They observed that the catalytically active sites are the metal ions in the structure. Furthermore, HKUST-1 exhibits high selectivity and yield for this reaction.[28] Camu and collaborators,[29] studied UiO-66 in the same reaction, obtaining a conversion of over 80%. Additionally, MOFs are structures that can be modified by incorporating functional groups in the ligand, which is observed in the presence of UiO-66-F, which considerably increases the conversion of the reaction due to the higher acidity of the material. Arrozi,[30] reported the use of UiO-66 and UiO-67 observing that the accessibility of the active sites can influence a higher conversion with respect to the Lewis acidity of the Zr-MOFs. Between the previously mentioned MOFs, MOF-808 has Lewis and Brønsted acid sites that have better accessibility in comparison with other MOFs, due to the smaller number of ligands in their structure.[31]

MOF-808-Zr is composed of an SBU with the chemical formula $(Zr_6O_4(OH)_4(-COO^-)_6)^{+6}$ bonded to six molecules of trimesic acid (benzene-1,3,5-tricarboxylic acid) as organic ligand.[32] MOF-808-Zr has been previously used as a catalyst in the acetalization of benzaldehyde with methanol with photothermal conditions.[31] There are reports of other isoreticular structures of MOF-808-Zr with metallic centers of Hf (IV),[33](MOF-808-Hf) and Ce(IV).[34]MOF-808-Ce that have not been studied in this application before.

Our work studied the influence of the metal center in MOF-808-M, where M are Zr(IV), Hf(IV) or Ce(IV). Furthermore, MOF-808-Ce showed the best catalytic activity, which exhibited high porosity and presents interesting redox properties.[35] The MOFs were prepared with the aim of understanding the metallic center influence over the methanol benzaldehyde acetalization catalytic activity. Furthermore, the three MOF-808-M derivatives were fully characterized by means of powder X-ray diffractometry, spectroscopy FT-IR, N_2 sorption, potentiometric acid–base titration, and thermogravimetric analysis. Also, DFT calculation of the MOF-808-M reduced model was performed to further support the experimentally observed catalytic results.

Experimental section

Materials and methods

Zirconium(IV) chloride anhydrous ($ZrCl_4$, 98%, Acros Organics), hafnium(IV) chloride ($ZrCl_4$, 99,9%, Strem Chemicals), cerium (IV) ammonium nitrate ($(NH_4)_2Ce(NO_3)_6$, 98,5%, Sigma Aldrich), benzene-1,3,5-tricarboxylic acid (H_3BTC, Merk, 98%), *N*,*N*-dimethylformamide (DMF, 99%, Merk), formic acid for analysis (HCOOH, 98–100%, Merk), benzaldehyde for synthesis (99%, Merck), methanol (99.5%, Merk), hydrochloric acid 37% for analysis (Winkler), sodium hydroxide pellets for analysis (99%, Merk), naphthalene (99%, Sigma Aldrich), sodium nitrate (99%, ACS reagent) and acetone (99%, Winkler) were used as obtained. PXRD characterization for product identification was performed on a D2 PHASER Bruker with Mo Kα1 radiation. For the textural determination, MOF-808-Zr and MOF-808-Hf were activated for 12 hours at 120 °C and MOF-808-Ce for 4 hours at 100 °C, under vacuum in a VACPREP 061. Sorption was performed using GEMINI VII, Micromeritics, with nitrogen as adsorbate. The specific areas were determined using the Brunauer–Emmett–Teller (BET) method and the pore size was obtained by pore diameter distribution using the Howart Kawazoe (HK) method. The Fourier transformed infrared spectroscopy (FT-IR) spectra were carried out with an attenuated reflectance accessory (ATR) in IRSpirit equipment, SHIMADZU. Thermogravimetric measurements were performed on TGA/SDTA851, Mettler-Toledo thermobalance, the sample was measured from 20 °C to 900 °C with a 20 °C min^{-1} slope using a constant flux of nitrogen. X-Ray Photoelectron Spectroscopy, XPS, was performed on the powder samples to obtain elemental composition, by using a Surface Analysis Station 1, model XPS RQ300/2, employing Al radiation (1486.6 eV) and an accelerated voltage of 15 kV. The scanning range was 1200–0 eV at a step size and step time of 1 eV and 0.2 s, respectively. The powdered samples were loaded onto double-sided sticky carbon tape and then mounted on the sample holder. The qualitative analysis and elemental assignment were performed using the CasaXPS software database.

Synthesis of MOF-808-Zr and MOF-808-Hf

The materials were synthesized according to the published literatures with a slight modification.[36,37] $ZrCl_4$ (0.2330 g; 1 mmol) was dissolved in a glass vial in 3.5 mL of DMF. In a second vial, the linker benzene-1,3,5-tricarboxylic acid (0.2101 g; 1 mmol) was dissolved in 3.5 mL of DMF. Both solutions were placed in a sonicator for 20 minutes. Subsequently, both vials were mixed and 7 mL of HCOOH were added. The mixture was heated at 100 °C for 24 hours. A powder white

solid was collected and washed three times with 6.0 mL of DMF and three times with 6.0 mL of acetone, each one performed every six hours. Finally, the material was dried at room temperature with vacuum in a desiccator. MOF-808-Hf was synthesized following the same procedure, using $HfCl_4$ instead of $ZrCl_4$.

Synthesis of MOF-808-Ce

The synthesis was realized based on the previous publications.[38] Benzene-1,3,5-tricarboxylic acid (0.064 g), DMF (3.4 mL) of DMF, and formic acid (734.28 μL) were added to a 20 mL glass reactor. Subsequently, an aqueous solution of ammonium cerium(IV) nitrate (1714 μL, 0.533 M) was added to the mixture. The glass reactor was sealed and heated for 15 min at 100 °C in a programmed oven. A powder yellow solid was collected and washed twice with 3.4 mL of DMF and four times with 3.4 mL of acetone. Finally, the material was dried at room temperature in a desiccator for 3 days.

Catalytic tests

The procedure of this essay was based on published literature with some adjustments.[29] Before the catalytic test, the materials MOF-808-Zr, MOF-808-Hf and MOF-808-Ce were activated using the same conditions indicated in the activation for the surface area measurements. The benzaldehyde acetalization was carried out at room temperature and without pressure in a glass reactor loaded with 10 mL of methanol, 35 mg of naphthalene as internal standard, 330 μL of benzaldehyde, and 13 mg of the respective catalyst, in this case, MOF-808-Zr and MOF-808-Hf. In the situation of MOF-808-Ce, the glass reactor was loaded with 20 mL of methanol, 35 mg of naphthalene as an internal standard, and 700 μL of benzaldehyde. The reaction conversion was monitored by taking aliquots at different time intervals to analyze by gas chromatography (GC) on a Shimadzu GC-2030 equipped with a flame ionization detector (FID). The values of reaction conversion were obtained according to ([A]/([A] + [Bz])) where [A] is de molar concentration of acetal produced and [Bz] is the molar concentration of benzaldehyde consumed.[24] For all materials, the mixture was stirred at 500 rpm for 180 minutes. To test the reusability of the catalyst, the used MOF was recovered and washed twice with 5 mL of acetone, followed by its subsequent drying in a non-vacuum oven to eliminate solvent excess (4 hours). When the recovered MOF is dry it is activated in a vacuum oven at 80 °C for 3 hours. After activation, the amount of MOF recovered was determined, low sizing the initial amounts of the acetalization reaction based on the new amount of starting material available. The intrinsic rate (r_i) due to defects present in the calculation materials according to $r_i = r/ND$, where r is the reaction rate obtained by the initial slope of a conversion *versus* time graph and ND the number of defects in the materials.[24]

Computational study

In this work for MOF-808-M a representative fragment is based on the secondary building unit (SBU), which consists of the fragments $[M_6O_4(OH)_4(H_3BTC)_5(HCOO)_6]^{+1}$ (M = Ce(IV), Zr(IV), and Hf(IV)). See ESI section 2.1† for more details. In MOFs, such as UiO series and MOF-808, Brønsted sites arise due to defect sites from missing linkers.[39,40] In the vacancy site, the coordination of $-OH_2$ and –OH groups compensate the charge imbalance due to a missing linker. Thus, enhancement accessibility of substrates in these acid sites (Metal–OH_2 and Metal–OH) of the node, which is very relevant in catalytic reactions I.[41,42] In these our cluster models was considered one defect site arising from a missing linker, see Fig. S8.† The crystal structure for MOF-808-Zr[43] was used as template to create the cluster model of MOF-808-Zr, MOF-808-Hf and MOF-808-Ce. From a theoretical standpoint it was explored the intermolecular interactions of benzaldehyde and methanol with the MOF-808-M. The calculations were conducted employing the DFT approach, as implemented in the Amsterdam Density Functional (ADF2019) software package.[44] The chemical and physical properties of heavy elements and their compounds are importantly influenced by relativistic effects. Therefore, to effectively handle these relativistic impacts in these systems, we integrate a zeroth-order regular approximation approach into the calculations.[45] In the first step, the geometry optimizations were performed using the generalized gradient approximation (GGA) with the Becke–Perdew (BP86) exchange–correlation functional[46] along with the standard Slater-type orbital (STO) basis set plus two-polarization functions (STO-TZ2P).[47]

In the second step, to explore the adsorption of benzaldehyde and methanol on the defect sites (arising from the missing linkers) of the MOF, the interaction energy (E_{Int}) was computed. The E_{Int} was calculated based on the energy of the optimized geometry of MOF-808-M/benzaldehyde and MOF-808-M/methanol systems and the energy of their fragments. The following equation, as previously reported,[48,49] was used to calculate the E_{Int}:

$$E_{Int} = E_{(MOF\text{-}808\text{-}M/guest)} - (E_{(MOF\text{-}808\text{-}M)} + E_{(guest)})$$

where $E_{(MOF\text{-}808\text{-}M/guest)}$ is the energy of the optimized MOF-808-M/benzaldehyde or MOF-808-M/methanol system, which is the total energy of the system when the two fragments are interacting. $E_{(MOF\text{-}808\text{-}M)} + E_{(guest)}$ are the energies of the individual fragments obtained during the optimization process (guest = benzaldehyde or methanol). And the E_{Int} is the interaction energy between the two fragments. Additionally, due to the existence of the basis set superposition error (BSSE), the interaction energies were corrected by using the counterpoise method.[50]

Results and discussion

MOFs characterization

The synthesized materials were characterized by different methods (Fig. 1). First, PXRD evaluated the structure and crystallinity of the MOFs. The presence of the MOF-808 structure could be confirmed by comparing the experimental patterns

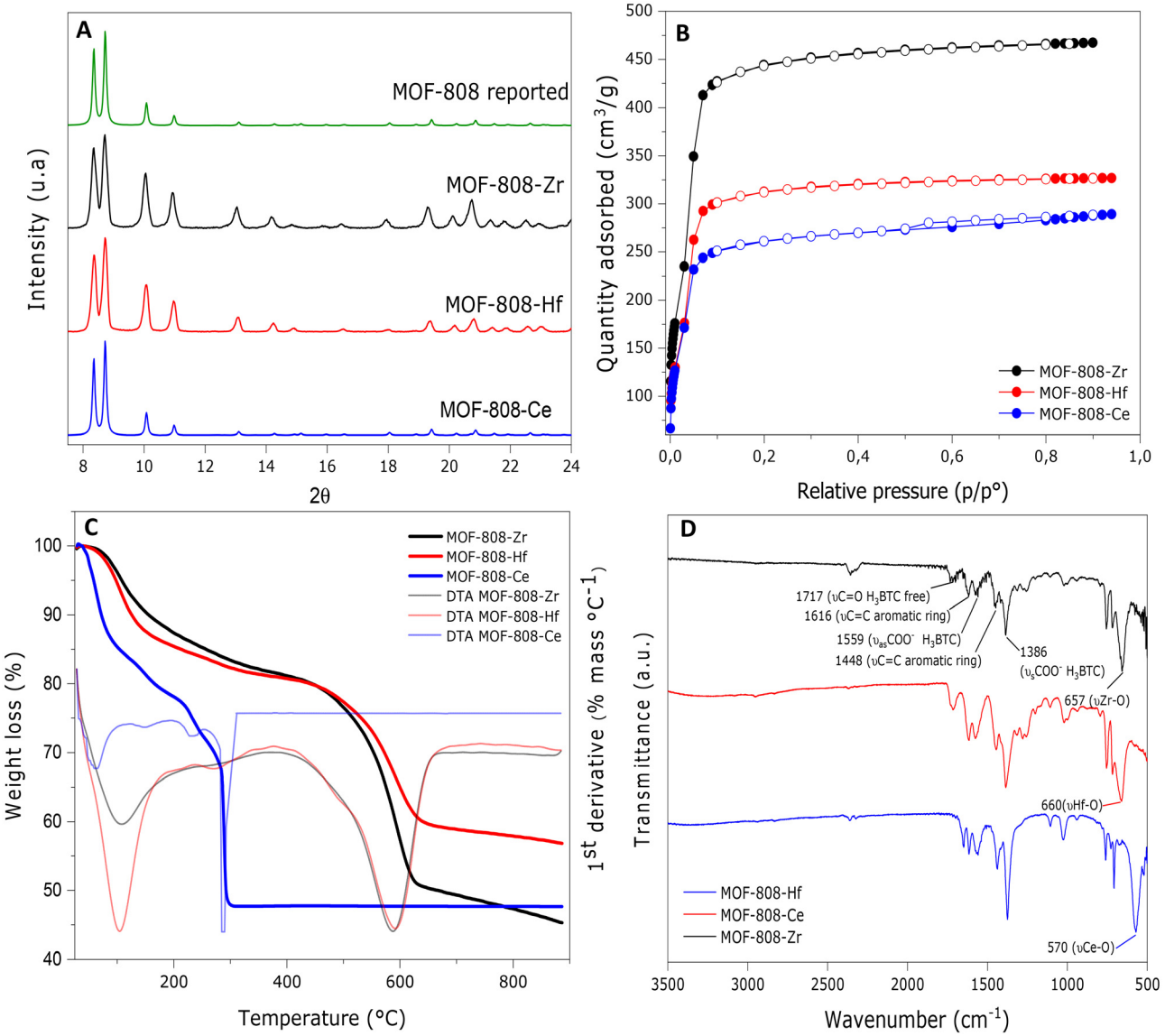

Fig. 1 Characterization obtained for MOF-808-Zr, MOF-808-Hf and MOF-808-Ce; (A) PXRD patterns; (B) TGA analysis; (C) nitrogen adsorption–desorption isotherm and (D) ATR-FTIR spectra.

with the previously reported structure pattern Fig. 1A. The absence of unknown peaks supports the pure crystallinity of materials, and the similarity of the patterns indicates that they have isoreticular structures. The textural properties of synthesized MOFs were evaluated by N_2 adsorption–desorption measurements. The N_2 isotherms for the studied systems are shown in Fig. 1B, where all the compounds exhibited Type I isotherms, characteristic of microporous materials according to IUPAC criteria.[51] The BET surface areas showed a decreasing tendency from MOF-808-Zr, MOF-808-Hf, and MOF-808-Ce with values of 1339, 958 and 812 $m^2\ g^{-1}$ and pore sizes of 8.0, 8.5 and 8.0 Å, respectively, all of them into the range of reported values of surface area.[52] The large observed pore size values (greater than 2 nm) are associated with the presence of defects in the structures. The thermic characterization of the studied system was realized through a thermogravimetric analysis (TGA), shown in Fig. 1C. MOF-808-Zr and MOF-808-Hf showed a similar behavior, exhibiting an initial mass loss in the range of 25 to 100 °C due to the desorption of physisorbed water in the materials. A second weight loss is observed at 160 °C, attributed to the loss of formic acid molecules trapped in the material. Finally, the third weight loss, associated with the degradation of the organic ligand and the decomposition of the MOF, is located at 590 °C, approximately.[29] On the other hand, the profile observed for the MOF-808-Ce has the same three mass losses observed in its analogues of Zr and Hf. The difference is in the temperature of the third weight loss that occurs in a minor value (286 °C), indicating that the MOF-808-Ce has a minor degradation temperature associated with the less force of the Ce–O bond in comparison with the Zr–O or

Hf–O bond.[53] The chemical structure of materials was confirmed by infrared spectroscopy whose results are the infrared spectra shown in Fig. 1D. The FT-IR spectra indicate the presence of different vibrational bands associated to the organic portion of the MOF and to the metal-linker bond. The bands located approximately at 1619 and 1448 cm^{-1} for the three materials are associated with the C=C vibrations of the aromatic ring. The vibrations between 1560 and 1386 cm^{-1} are associated with asymmetric and symmetric vibration of the carboxylic groups (COO^{-}), respectively. Finally, the band associated with the metal–oxygen interactions is observed below 600 cm^{-1}, specifically at 657, 660 and 570 cm^{-1} for MOF-808-Zr, MOF-808-Hf and MOF-808-Ce, respectively. These values support the energy difference between M–O bonds, where high values indicate a high energy bond.[53]

To characterize the structure of the SBU in these MOFs and their reactivity, potentiometric titration (PT) was performed. The full set of results is shown in ESI.† By means of the PT, four equivalence points were obtained for the synthesized materials. The first three equivalence points are associated with μ_3–OH, M–OH_2 and M–OH, respectively, with characteristic pK_a values, see Table S1 and Fig. S1A, S1B.† Furthermore, the three synthesized materials present a fourth equivalence point that, to the best of our knowledge, has not been discussed before. The shown results support the MOF breakdown after the PT process.[54] Using the obtained results by potentiometric titration, as has been previously reported,[55] it was possible to determine the defects present in each synthesized structure. Specifically, MOF-808-Zr and MOF-808-Hf showed 0.39 defects, whereas MOF-808-Ce showed 0.87 defects. Thus, MOF-808-Ce has a greater number of defects with respect to MOF-808-Zr and MOF-808-Hf. This result supports the fact that the Ce–O bond is more labile than Zr–O and Hf–O bond. Finally, it should also be considered that a larger number of defects is associated with the presence of more Lewis acid sites, as observed in MOF-808-Ce, see Table S2.†

Scanning electron microscopy (SEM) was used to obtain information on the crystal morphology of the synthesized materials, see Fig. 2. As could be observed, all the studied materials showed an octahedral particle morphology, with a diameter between 100 and 800 nm, with a reduced size for MOF-808-Ce. By means of EDS (see Fig. S7, S8 and S9†), it was possible to observe the presence of Zr, Hf and Ce atoms in each of the materials. Also, the presence of O and C atoms, mostly attributed to the organic ligand H_3BTC, are also observed.

Based on the XPS analysis of the MOF-808-Ce catalyst, the spectra corresponding to the Ce 3d elements found in the material's structure are displayed in Fig. 3. The deconvolution of the Ce 3d spectrum suggests the presence of 10 peaks. Three peaks for Ce(IV) $3d_{5/2}$ are shown to be present at 882.1, 886.7, and 897.9 eV, whereas three peaks for Ce(IV) $3d_{3/2}$ are seen to be present at 900.7, 906.0, and 916.3 eV. On the other hand, Ce(III) produces four peaks at eV 880.5, 884.7, 899.3, and 903.4.[56] Based on the peak region of the deconvoluted core level spectra, it was found that MOF-808-Ce contained 54.9% of the relative quantity of Ce(III) and 45.1% of Ce(IV) (Table 1). The reducing capacity of the DMF solvent with a lengthy reaction time at high temperatures, on the other hand, is what causes the existence of Ce(III). Ce(IV) partially forms Ce(III)[57] as a result of the electron's preferential gain due to the low energy difference nature of the empty 4f band of Ce in MOF-808-Ce. Light-metal charge transfer and photon absorption may be enhanced by the Ce(IV)/Ce(III) orbitals combined

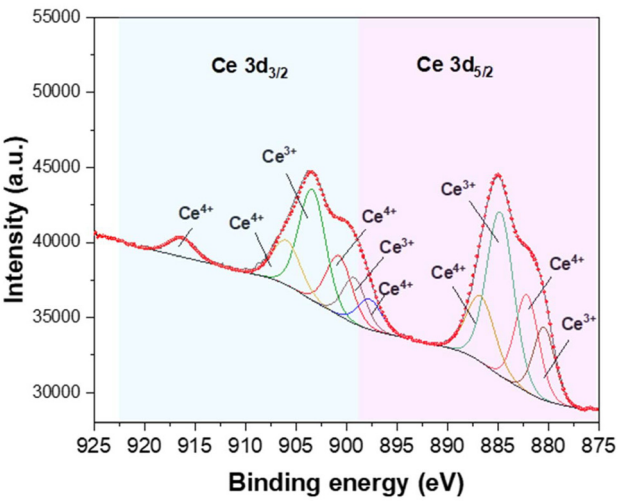

Fig. 3 XPS analysis MOF-808-Ce.

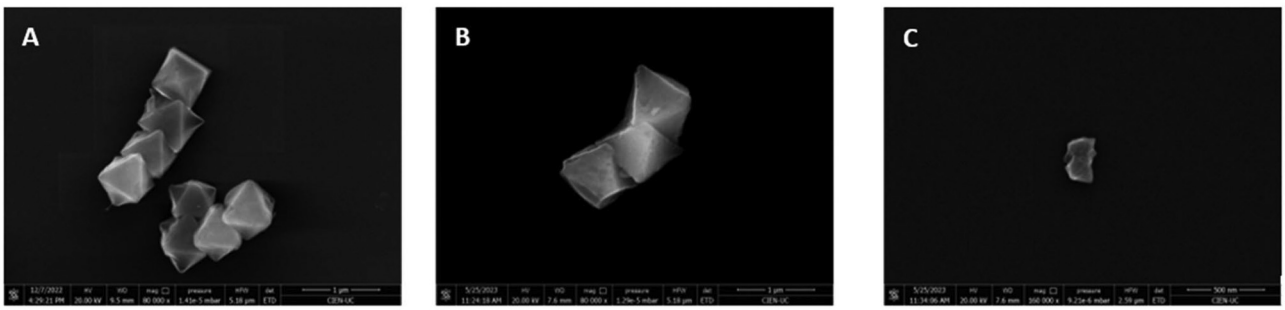

Fig. 2 SEM images of MOF-808-Zr (A); MOF-808-Hf (B) and MOF-808-Ce (C).

Table 1 Percentage of Ce(III) and Ce(IV) in MOF-808 and their ratio

#	Catalyst	Ce 3d fraction (%)		Atomic ratio Ce3+/Ce4+
		Ce(III)	Ce(IV)	
1	MOF-808-Ce	54.9	45.1	0.82

with the organic ligand orbitals.[57] The presence of trivalent cerium on the MOF-808-Ce structure could explain the low thermic stability of this material because the Ce(III) atoms break the octahedral Ce(IV) that forms the characteristic SBU of MOF-808.[58]

Additionally, potentiometric titration with *n*-butylamine, described in literature,[59] was carried out to determine the acid strength of the MOFs by the initial electrode potential. In the case of MOF-808-Ce the initial electrode potential was 128 mV, therefore this material has very strong acid sites. On the other hand, the MOF-808-Zr and MOF-808-Hf have an initial electrode potential of −37 mV and −28 mV, which indicates the presence of weak acid sites (Fig. 4). Additionally, with the total number of acid sites and the specific surface area is possible to determine each material's acid site density. Thereby, it was obtained that MOF-808-Ce has a larger acid site density, with a value of 4.5×10^{-3} meq m^{-2}, than its homologs of Zr and Hf with values of 2.13×10^{-3} and 1.82×10^{-3} meq m^{-2}, respectively.

Catalytic activities

After the synthesized materials were characterized, the catalytic evaluation was done over the acetalization reaction of benzaldehyde with methanol (with no temperature and no pressure). Fig. 5A shows that MOF-808-Ce presents conversions from benzaldehyde to (dimethoxymethyl)benzene with values greater than 80% after 10 minutes of reaction. Otherwise, for MOF-808-Zr and MOF-808-Hf, a conversion of 3% after three hours of reaction was observed. Thus, the influence on the studied catalytic activity might be associated to the presence of defects in the structure and its acidic properties.

Under the same reaction conditions MOF-808-Ce showed high catalytic activity with respect to the rest of the materials. After 5 minutes of reaction MOF-808-Ce showed 100% conversion or total consumption of benzaldehyde (see ESI Fig. S5†). To study with better precision the catalytic behavior of this

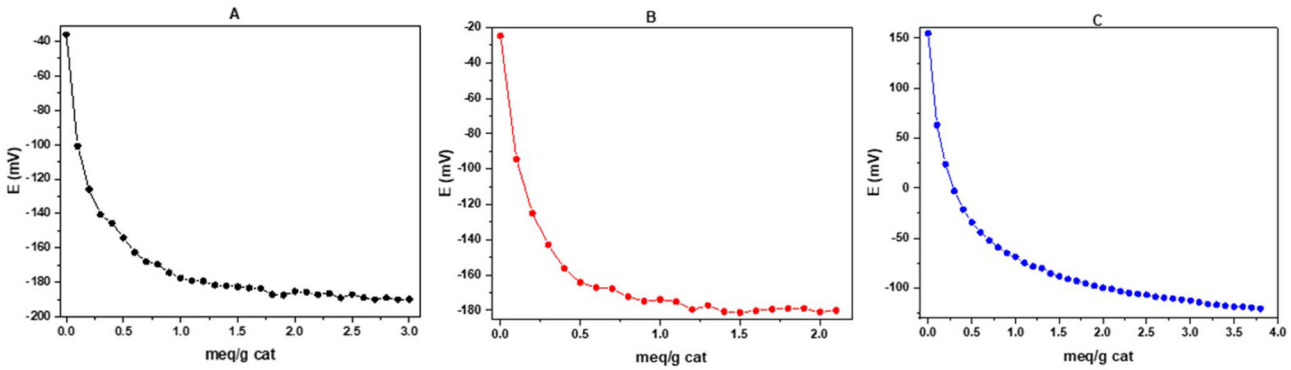

Fig. 4 Potentiometric titration curve with butilamina in acetonitrile of MOF-808-Zr (A), MOF-808-Hf (B) and MOF-808-Ce (C).

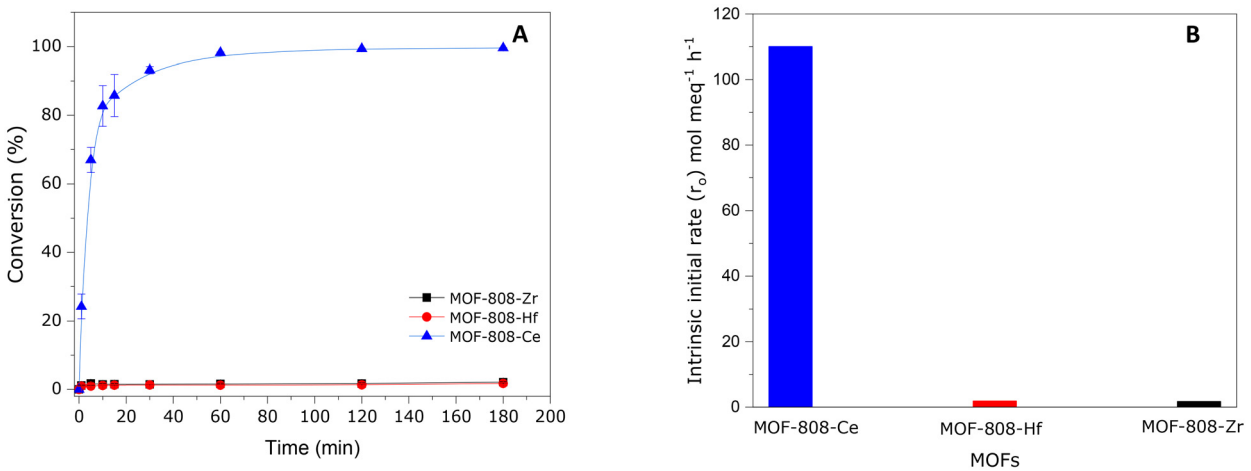

Fig. 5 Conversion *versus* time in the acetalization of benzaldehyde with methanol catalyzed by MOF-808-Zr, MOF-808-Hf and MOF-808-Ce (A), intrinsic initial rate for MOF-808-Zr, MOF-808-Hf and MOF-808-Ce normalizing by ASD (B).

material, twice the concentration of benzaldehyde was used to saturate the active sites of the material and decrease the initial reaction rate. Finally, the catalytic activities are shown normalized by the mass of catalyst, mass as a function of benzaldehyde decomposition, making the catalytic experiments comparable.

To understand this behavior, it was necessary to calculate the values of intrinsic initial rate (r_o), obtained from the slope of the initial values of the conversion curve, and normalizing the acquiring data with the acidic sites density (ASD). In this case, it is obtained (see Fig. 5b) that MOF-808-Ce has 109.9 mol meq^{-1} h^{-1}, MOF-808-Zr 1.69 mol meq^{-1} h^{-1} and MOF-808-Hf 1.82 mol meq^{-1} h^{-1}. This result supports the high conversion obtained for the MOF-808-Ce, as it has very strong acid sites and a larger acid site density, compared to the other two studied materials. Furthermore, the MOF-808-Zr and MOF-808-Hf have similar acid site density and acid sites with similar strength which justifies their similar catalytic conversion. It is important to stand out that the existence of weak acid sites in a low density in the MOF-808-Hf explains the low conversion obtained, an expected result in comparison with the reported literature.[60] Furthermore, by normalizing the initial rate by acid strength and defects in each of the materials, it is observed that in every case MOF-808-Ce has a higher initial intrinsic rate. Therefore, its greater conversion is also influenced by the greater number of defects present in the material and the greater acid force existing in the structure (see ESI Fig. S10 and S11†). In fact, it is probable that for this reaction a cooperative effect between acid site density, acid strength and structural defects exist for each material, being more remarkable for the case of MOF-808-Ce.

Due to the high conversion shown by MOF-808-Ce, recovery and reuse were evaluated only for this material (Fig. 6). As can be seen, after four catalytic cycles, the MOF loses its activity, decreasing from 100% activity to 1.5%. After the catalytic recycle, the used MOF was characterized with a PXRD, FT-IR spectroscopy and N_2 isotherms (Fig. S2, S3 and S4†) where the results indicate a loss of crystallinity of MOF-808-Ce and a decrease in its BET surface reduced to 283 m^2 g^{-1} that can be associated to the loss of activity of the MOF. Furthermore, an increase in pore size by BJH method was observed at 4.7 nm, which is attributed to the loss of material integrity.

Furthermore, the recovered MOF-808-Ce after catalytic recycling was subjected to potentiometric titration with *n*-butylamine. The initial electrode potential was determined to be 65 mV, thus the strength of acid sites decreases after reuse. The density of acid sites also decreases to a value of 2.5 × 10^{-3} meq m^{-2} (see ESI Fig. S6†). Both factors could explain the drop-in material activity in the recycles.

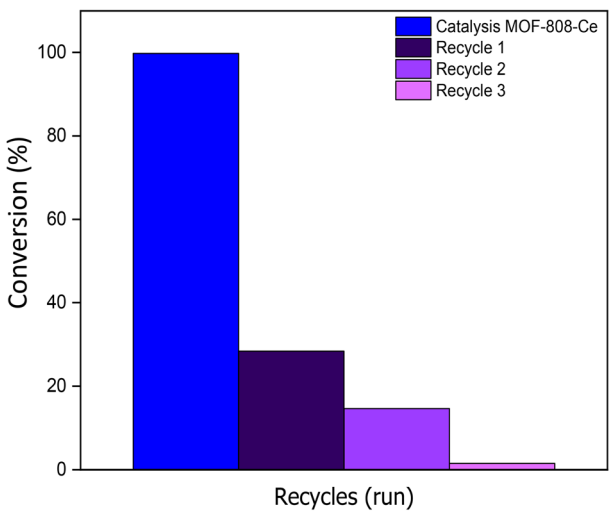

Fig. 6 Recyclable results of MOF-808-Ce catalyzed acetalization of benzaldehyde.

Computational analysis

To gain a deeper understanding of the benzaldehyde and methanol interactions role on the MOF-808-M systems, the interaction energy (E_{int}) was computed. In the first sept, the interacting systems MOF-808-M/benzaldehyde and MOF-808-M/methanol were optimized in their ground electronic state (S_0). As it can be seen in section 2.2 in the ESI.† The E_{Int} was calculated considering the energy of the optimized interacting MOF systems and the energy of the separated fragments (*i.e.* MOF-808-M and guest) (benzaldehyde and methanol, respectively). The interaction energy is a key parameter that provides information about the interactions (both covalent and non-covalent) that take place in the interacting system, host–guest.[48]

As shown in Table 2, the E_{Int} suggests that the interaction of MOF-808-Hf (−25.20 kcal mol^{-1}) and MOF-808-Zr (−24.29 kcal mol^{-1}) with benzaldehyde is stronger than the interaction between MOF-808-Ce and benzaldehyde (E_{int} = −20.67 kcal mol^{-1}). Considering that more negative energy values result in stronger interactions.[48] The same trend is observed for the interaction between MOF-808-M and methanol, for all three materials. This lower energy E_{Int} for MOF-808-Ce/guest systems provides evidence that the adsorption of benzaldehyde and methanol on the defect sites are weaker, compared to the other two materials. It has been previously reported, that for a heterogeneous catalyst to be most active, the appropriate substrate adsorption energy should be measured. Thus, when a weak adsorption energy is obtained, the catalyst is not effective, due to low interactions with the substrate. On the other hand, if a strong interaction is found, the catalyst is also not effective, due to poisoning, or strong adsorption of the substrate over the

Table 2 Interaction distances MOF-808-M/benzaldehyde and MOF-808-M/methanol (Å), interaction energy (kcal mol^{-1})

Host-gest system	Intermolecular distances	E_{Int}
MOF-808-Hf/benzaldehyde	2.48	−25.20
MOF-808-Zr/benzaldehyde	2.47	−24.29
MOF-808-Ce/benzaldehyde	2.60	−20.67
MOF-808-Hf/methanol	2.52	−23.52
MOF-808-Zr/methanol	2.62	−22.76
MOF-808-Ce/methanol	2.68	−20.17

active site. In our case, we propose that this situation is observed. In this sense, in the case of MOF-808-Ce the adsorption step of benzaldehyde and methanol has the appropriate energy for the substrate/catalyst interaction, resulting in higher conversion observed experimentally. Whereas the MOF-808-Zr and MOF-808-Hf show a strong adsorption energy, which does not favour (in this case) the catalytic activity of the studied MOFs. This leads us to believe that in the case of MOF-808-Ce the dissociation step of benzaldehyde and methanol is easier, resulting in higher conversion observed experimentally, see ESI† for further discussion.

Conclusions

It was possible to synthesize MOF-808-Zr, MOF-808-Hf and MOF-808-Ce by solvothermal synthesis. The products obtained were characterized structurally and texturally. Subsequently, the catalytic activity in the acetalization reaction of benzaldehyde with methanol was evaluated. It is observed that MOF 808 Ce is the material that presented a higher conversion compared to the other materials, which is also observed in the initial intrinsic velocity values obtained through normalization by density of acid sites, where r_o in MOF-808-Ce is 109.9 (mol meq^{-1} h^{-1}), while its Zr and Hf analogues present r_o values of 1.69 and 1.82 (mol meq^{-1} h^{-1}), respectively. Therefore, the high conversion of MOF-808-Ce is influenced by the higher presence of acid density in this material. The reutilization of MOF-808-Ce shows a loss of its catalytic activity that can be associated with the loss of the integrity of material shown through a loss of crystallinity and superficial area of material characterized after the first catalytic recycle. Computational analysis has shed light on the role of the strength of interactions of the substrate in the defect sites (arising from missing linkers) of material into the conversion of benzaldehyde to (dimethoxymethyl) benzene This property of MOF-808-Ce could be exploited in applications where higher conversion rates are desirable. This knowledge can guide the rational designing of MOFs with tailored properties, thereby opening new avenues in the realm of material science and catalysis.

Data availability

The data supporting this article have been included as part of the ESI.†

Conflicts of interest

There are no conflicts to declare.

Acknowledgements

The authors thank FONDECYT 1231194, 1241917 and ANID Postdoctoral 3230141 This work was funded by ANID-Millennium Science Initiative Program-NCN21_90. ANID/FONDAP/1523A0006. ACT210057.

References

1 S. Dutta and S. Pal, Promises in Direct Conversion of Cellulose and Lignocellulosic Biomass to Chemicals and Fuels: Combined Solvent–Nanocatalysis Approach for Biorefinary, *Biomass Bioenergy*, 2014, **62**, 182–197, DOI: **10.1016/j.biombioe.2013.12.019**.

2 A. Hornung, *Transformation of Biomass*, ed. A. Hornung, John Wiley & Sons, Ltd, Chichester, UK, 2014. DOI: **10.1002/9781118693643**.

3 D. Esposito and M. Antonietti, Redefining Biorefinery: The Search for Unconventional Building Blocks for Materials, *Chem. Soc. Rev.*, 2015, **44**(16), 5821–5835, DOI: **10.1039/C4CS00368C**.

4 P. Gallezot, Conversion of Biomass to Selected Chemical Products, *Chem. Soc. Rev.*, 2012, **41**(4), 1538–1558, DOI: **10.1039/C1CS15147A**.

5 S. Fernando, S. Adhikari, C. Chandrapal and N. Murali, Biorefineries: Current Status, Challenges, and Future Direction, *Energy Fuels*, 2006, **20**(4), 1727–1737, DOI: **10.1021/ef060097w**.

6 J.-P. Lange, Lignocellulose Conversion: An Introduction to Chemistry, Process and Economics, *Biofuels, Bioprod. Biorefin.*, 2007, **1**(1), 39–48, DOI: **10.1002/bbb.7**.

7 Y.-H. P. Zhang, Reviving the Carbohydrate Economy via Multi-Product Lignocellulose Biorefineries, *J. Ind. Microbiol. Biotechnol.*, 2008, **35**(5), 367–375, DOI: **10.1007/s10295-007-0293-6**.

8 I. S. Goldstein, *Pyrolysis in Organic Chemicals from Biomass*, CRC Press, Boca Raton, 1981.

9 P. McKendry, Energy Production from Biomass (Part 1): Overview of Biomass, *Bioresour. Technol.*, 2002, **83**(1), 37–46, DOI: **10.1016/S0960-8524(01)00118-3**.

10 A. Bridgwater, S. Czernik and J. Piskorz, An Overview of Fast Pyrolysis, in *Progress in Thermochemical Biomass Conversion*, Blackwell Science Ltd, Oxford, UK, 2008, vol. 30, pp. 977–997. DOI: **10.1002/9780470694954.ch80**.

11 S. Wang, Z. Wan, Y. Han, Y. Jiao, Z. Li, P. Fu, N. Li, A. Zhang and W. Yi, A Review on Lignin Waste Valorization by Catalytic Pyrolysis: Catalyst, Reaction System, and Industrial Symbiosis Mode, *J. Environ. Chem. Eng.*, 2023, 109113, DOI: **10.1016/j.jece.2022.109113**.

12 S. Zhao, Y. Jia and Y. F. Song, Acetalization of Aldehydes and Ketones over H4[SiW 12O40] and H4[SiW12O 40]/SiO_2, *Catal. Sci. Technol.*, 2014, **4**(8), 2618–2625, DOI: **10.1039/c4cy00021h**.

13 Y. Wang, D. Jiang and L. Dai, Novel Brønsted Acidic Ionic Liquids Based on Benzimidazolium Cation: Synthesis and Catalyzed Acetalization of Aromatic Aldehydes with Diols, *Catal. Commun.*, 2008, **9**(15), 2475–2480, DOI: **10.1016/j.catcom.2008.06.021**.

14 M. J. Climent, A. Velty and A. Corma, Design of a Solid Catalyst for the Synthesis of a Molecule with Blossom Orange Scent, *Green Chem.*, 2002, **4**(6), 565–569, DOI: 10.1039/b207506g.
15 H.-C. "Joe" Zhou and S. Kitagawa, Metal–Organic Frameworks (MOFs), *Chem. Soc. Rev.*, 2014, **43**(16), 5415–5418, DOI: 10.1039/C4CS90059F.
16 A. Corma, H. García and F. X. Llabrés i Xamena, Engineering Metal Organic Frameworks for Heterogeneous Catalysis, *Chem. Rev.*, 2010, **110**(8), 4606–4655, DOI: 10.1021/cr9003924.
17 Q. Shen, X. Li, R. Li and Y. Wu, Application of Metal–Organic Framework Materials and Derived Porous Carbon Materials in Catalytic Hydrogenation, *ACS Sustainable Chem. Eng.*, 2020, **8**(48), 17608–17621, DOI: 10.1021/acssuschemeng.0c06849.
18 H. Li, K. Wang, Y. Sun, C. T. Lollar, J. Li and H.-C. Zhou, Recent Advances in Gas Storage and Separation Using Metal–Organic Frameworks, *Mater. Today*, 2018, **21**(2), 108–121, DOI: 10.1016/j.mattod.2017.07.006.
19 A. Schoedel and S. Rajeh, Why Design Matters: From Decorated Metal Oxide Clusters to Functional Metal–Organic Frameworks, *Top. Curr. Chem.*, 2020, **378**(1), 19, DOI: 10.1007/s41061-020-0281-0.
20 A. J. Howarth, A. W. Peters, N. A. Vermeulen, T. C. Wang, J. T. Hupp and O. K. Farha, Best Practices for the Synthesis, Activation, and Characterization of Metal–Organic Frameworks, *Chem. Mater.*, 2017, **29**(1), 26–39, DOI: 10.1021/acs.chemmater.6b02626.
21 V. V. Butova, M. A. Soldatov, A. A. Guda, K. A. Lomachenko and C. Lamberti, Metal-Organic Frameworks: Structure, Properties, Methods of Synthesis and Characterization, *Russ. Chem. Rev.*, 2016, **85**(3), 280–307, DOI: 10.1070/rcr4554.
22 A. Dhakshinamoorthy, M. Alvaro and H. Garcia, Metal Organic Frameworks as Solid Acid Catalysts for Acetalization of Aldehydes with Methanol, *Adv. Synth. Catal.*, 2010, **352**(17), 3022–3030, DOI: 10.1002/adsc.201000537.
23 C. G. Piscopo, M. Schwarzer, M. Herrmann, A. Affini, P. Pelagatti, G. Maestri, R. Maggi and S. Loebbecke, Batch versus Flow Acetalization of Benzaldehyde with HKUST-1: Diffusion Pathways and Performance Comparison, *ChemCatChem*, 2016, **8**(7), 1293–1297, DOI: 10.1002/cctc.201501364.
24 E. Camu, C. Pazo, D. Becerra, Y. Hidalgo-Rosa, D. Paez-Hernandez, X. Zarate, E. Schott and N. Escalona, A New Approach to the Mechanism for the Acetalization of Benzaldehyde over MOF Catalysts, *New J. Chem.*, 2020, **44**(35), 14865–14871, DOI: 10.1039/d0nj02416c.
25 M. N. Timofeeva, V. N. Panchenko, J. W. Jun, Z. Hasan, M. M. Matrosova and S. H. Jhung, Effects of Linker Substitution on Catalytic Properties of Porous Zirconium Terephthalate UiO-66 in Acetalization of Benzaldehyde with Methanol, *Appl. Catal., A*, 2014, **471**, 91–97, DOI: 10.1016/j.apcata.2013.11.039.
26 U. S. F. Arrozi, H. W. Wijaya, A. Patah and Y. Permana, Efficient Acetalization of Benzaldehydes Using UiO-66 and UiO-67: Substrates Accessibility or Lewis Acidity of Zirconium, *Appl. Catal., A*, 2015, **506**, 77–84, DOI: 10.1016/j.apcata.2015.08.028.
27 R. C. Klet, Y. Liu, T. C. Wang, J. T. Hupp and O. K. Farha, Evaluation of Brønsted Acidity and Proton Topology in Zr- and Hf-Based Metal–Organic Frameworks Using Potentiometric Acid–Base Titration, *J. Mater. Chem. A*, 2016, **4**(4), 1479–1485, DOI: 10.1039/C5TA07687K.
28 A. Dhakshinamoorthy, M. Alvaro and H. Garcia, Metal Organic Frameworks as Solid Acid Catalysts for Acetalization of Aldehydes with Methanol, *Adv. Synth. Catal.*, 2010, **352**(17), 3022–3030, DOI: 10.1002/adsc.201000537.
29 E. Camu, C. Pazo, D. Becerra, Y. Hidalgo-Rosa, D. Paez-Hernandez, X. Zarate, E. Schott and N. Escalona, A New Approach to the Mechanism for the Acetalization of Benzaldehyde over MOF Catalysts, *New J. Chem.*, 2020, **44**(35), 14865–14871, DOI: 10.1039/d0nj02416c.
30 U. S. F. Arrozi, H. W. Wijaya, A. Patah and Y. Permana, Efficient Acetalization of Benzaldehydes Using UiO-66 and UiO-67: Substrates Accessibility or Lewis Acidity of Zirconium, *Appl. Catal., A*, 2015, **506**, 77–84, DOI: 10.1016/j.apcata.2015.08.028.
31 A. M. Rabon, J. G. Doremus and M. C. Young, MOF-808 as a Recyclable Catalyst for the Photothermal Acetalization of Aromatic Aldehydes, *Tetrahedron*, 2021, **85**, 132036, DOI: 10.1016/j.tet.2021.132036.
32 H. Furukawa, F. Gándara, Y.-B. Zhang, J. Jiang, W. L. Queen, M. R. Hudson and O. M. Yaghi, Water Adsorption in Porous Metal–Organic Frameworks and Related Materials, *J. Am. Chem. Soc.*, 2014, **136**(11), 4369–4381, DOI: 10.1021/ja500330a.
33 S. Rojas-Buzo, P. García-García and A. Corma, Catalytic Transfer Hydrogenation of Biomass-Derived Carbonyls over Hafnium-Based Metal-Organic Frameworks, *ChemSusChem*, 2018, **11**(2), 432–438, DOI: 10.1002/cssc.201701708.
34 M. Lammert, C. Glißmann, H. Reinsch and N. Stock, Synthesis and Characterization of New Ce(IV)-MOFs Exhibiting Various Framework Topologies, *Cryst. Growth Des.*, 2017, **17**(3), 1125–1131, DOI: 10.1021/acs.cgd.6b01512.
35 J. Jacobsen, A. Ienco, R. D'Amato, F. Costantino and N. Stock, The Chemistry of Ce-Based Metal-Organic Frameworks, *Dalton Trans.*, 2020, **49**(46), 16551–16586, DOI: 10.1039/d0dt02813d.
36 M. Li, J. Chen, W. Wu, Y. Fang and S. Dong, Oxidase-like MOF-818 Nanozyme with High Specificity for Catalysis of Catechol Oxidation, *J. Am. Chem. Soc.*, 2020, **142**(36), 15569–15574, DOI: 10.1021/jacs.0c07273.
37 Z. Hu, T. Kundu, Y. Wang, Y. Sun, K. Zeng and D. Zhao, Modulated Hydrothermal Synthesis of Highly Stable MOF-808(Hf) for Methane Storage, *ACS Sustainable Chem. Eng.*, 2020, **8**(46), 17042–17053, DOI: 10.1021/acssuschemeng.0c04486.

38 M. Lammert, C. Glißmann, H. Reinsch and N. Stock, Synthesis and Characterization of New Ce(IV)-MOFs Exhibiting Various Framework Topologies, *Cryst. Growth Des.*, 2017, **17**(3), 1125–1131, DOI: **10.1021/acs.cgd.6b01512**.

39 Y. Liu, R. C. Klet, J. T. Hupp and O. Farha, Probing the Correlations between the Defects in Metal-Organic Frameworks and Their Catalytic Activity by an Epoxide Ring-Opening Reaction, *Chem. Commun.*, 2016, **52**(50), 7806–7809, DOI: **10.1039/c6cc03727e**.

40 Z. Zhao, R. Lei, Y. Zhang, T. Cai and B. Han, Defect Controlled MOF-808 for Seawater Uranium Capture with High Capacity and Selectivity, *J. Mol. Liq.*, 2022, **367**, 120514, DOI: **10.1016/j.molliq.2022.120514**.

41 C. Pazo-Carballo, E. Blanco, E. Camu, A. Leiva, Y. Hidalgo-Rosa, X. Zarate, A. B. Dongil, E. Schott and N. Escalona, Theoretical and Experimental Study for Cross-Coupling Aldol Condensation over Mono- and Bimetallic UiO-66 Nanocatalysts, *ACS Appl. Nano Mater.*, 2023, **6**(7), 5422–5433, DOI: **10.1021/acsanm.2c05555**.

42 G. Ye, L. Wan, Q. Zhang, H. Liu, J. Zhou, L. Wu, X. Zeng, H. Wang, X. Chen and J. Wang, Boosting Catalytic Performance of MOF-808(Zr) by Direct Generation of Rich Defective Zr Nodes via a Solvent-Free Approach, *Inorg. Chem.*, 2023, **62**(10), 4248–4259, DOI: **10.1021/acs.inorgchem.2c04364**.

43 C. A. Trickett, T. M. Osborn Popp, J. Su, C. Yan, J. Weisberg, A. Huq, P. Urban, J. Jiang, M. J. Kalmutzki, Q. Liu, J. Baek, M. P. Head-Gordon, G. A. Somorjai, J. A. Reimer and O. M. Yaghi, Identification of the Strong Brønsted Acid Site in a Metal–Organic Framework Solid Acid Catalyst, *Nat. Chem.*, 2019, **11**(2), 170–176, DOI: **10.1038/s41557-018-0171-z**.

44 G. Te Velde, F. M. Bickelhaupt, E. J. Baerends, C. Fonseca Guerra, S. J. A. van Gisbergen, J. G. Snijders and T. Ziegler, Chemistry with ADF, *J. Comput. Chem.*, 2001, **22**(9), 931–967, DOI: **10.1002/jcc.1056**.

45 E. Van Lenthe, E. J. Baerends, J. G. Snijders, E. Van Lenthe, E. J. Baerends and J. G. Snijders, Relativistic Regular Twocomponent Hamiltonians Relativistic Regular Two-Component Hamiltonians, *J. Chem. Phys.*, 1993, **99**(6), 4597–4610, DOI: **10.1063/1.466059**.

46 J. P. Perdew and W. Yue, Accurate and Simple Density Functional for the Electronic Exchange Energy: Generalized Gradient Approximation, *Phys. Rev. B: Condens. Matter Mater. Phys.*, 1986, **33**(12), 8800–8802, DOI: **10.1103/PhysRevB.33.8800**.

47 E. Van Lenthe and E. J. Baerends, Optimized Slater-Type Basis Sets for the Elements 1-118, *J. Comput. Chem.*, 2003, **24**(9), 1142–1156, DOI: **10.1002/jcc.10255**.

48 N. V. Suresh Kumar and L. Srinivasa Rao, Theoretical Insights into Interaction Energy, IR Intensity and Raman Activity Enhancements of H_2O Adsorbed on Mg Containing Zn3O3 Nanoclusters: A Computational Study, *Comput. Theor. Chem.*, 2022, **1212**, 113708, DOI: **10.1016/j.comptc.2022.113708**.

49 K. Granados-Tavera, M. Zambrano-Angulo, Y. Hidalgo-Rosa, X. Zarate and G. Cárdenas-Jirón, Tuning the Visible-NIR Absorption of Azulenocyanine-Based Photosensitizers, *J. Mol. Model*, 2022, **28**(11), 1–13, DOI: **10.1007/S00894-022-05329-Y/TABLES/5**.

50 S. F. Boys and F. Bernardi, The Calculation of Small Molecular Interactions by the Differences of Separate Total Energies. Some Procedures with Reduced Errors, *Mol. Phys.*, 1970, **19**(4), 553–566, DOI: **10.1080/00268977000101561**.

51 M. Thommes, K. Kaneko, A. V. Neimark, J. P. Olivier, F. Rodriguez-Reinoso, J. Rouquerol and K. S. W. Sing, Physisorption of Gases, with Special Reference to the Evaluation of Surface Area and Pore Size Distribution (IUPAC Technical Report), *Pure Appl. Chem.*, 2015, **87**(9–10), 1051–1069, DOI: **10.1515/pac-2014-1117**.

52 Z. Hu, T. Kundu, Y. Wang, Y. Sun, K. Zeng and D. Zhao, Modulated Hydrothermal Synthesis of Highly Stable MOF-808(Hf) for Methane Storage, *ACS Sustainable Chem. Eng.*, 2020, **8**(46), 17042–17053, DOI: **10.1021/acssuschemeng.0c04486**.

53 V. R. Bakuru, S. R. Churipard, S. P. Maradur and S. B. Kalidindi, Exploring the Brønsted Acidity of UiO-66 (Zr, Ce, Hf) Metal–Organic Frameworks for Efficient Solketal Synthesis from Glycerol Acetalization, *Dalton Trans.*, 2019, **48**(3), 843–847, DOI: **10.1039/C8DT03512A**.

54 C. A. Trickett, T. M. Osborn Popp, J. Su, C. Yan, J. Weisberg, A. Huq, P. Urban, J. Jiang, M. J. Kalmutzki, Q. Liu, J. Baek, M. P. Head-Gordon, G. A. Somorjai, J. A. Reimer and O. M. Yaghi, Identification of the Strong Brønsted Acid Site in a Metal–Organic Framework Solid Acid Catalyst, *Nat. Chem.*, 2019, **11**(2), 170–176, DOI: **10.1038/s41557-018-0171-z**.

55 R. C. Klet, Y. Liu, T. C. Wang, J. T. Hupp and O. K. Farha, Evaluation of Brønsted Acidity and Proton Topology in Zr- and Hf-Based Metal-Organic Frameworks Using Potentiometric Acid-Base Titration, *J. Mater. Chem. A*, 2016, **4**(4), 1479–1485, DOI: **10.1039/c5ta07687k**.

56 G. Zhou, Y. Yao, X. Zhao, X. Liu, B. Sun and A. Zhou, Band Gap Energies for White Nanosheets/Yellow Nanoislands/Purple Nanorods of CeO_2, *RSC Adv.*, 2016, **6**(64), 59370–59374, DOI: **10.1039/C6RA11553E**.

57 H. Fei, J. Shin, Y. S. Meng, M. Adelhardt, J. Sutter, K. Meyer and S. M. Cohen, Reusable Oxidation Catalysis Using Metal-Monocatecholato Species in a Robust Metal–Organic Framework, *J. Am. Chem. Soc.*, 2014, **136**(13), 4965–4973, DOI: **10.1021/ja411627z**.

58 Z. Hu, Y. Wang and D. Zhao, The Chemistry and Applications of Hafnium and Cerium(Iv) Metal-Organic Frameworks, *Chem. Soc. Rev.*, 2021, 4629–4683, DOI: **10.1039/d0cs00920b**.

59 R. Cid and G. Pecchi, Potentiometric Method for Determining the Number and Relative Strength of Acid Sites in Colored Catalysts, *Appl. Catal.*, 1985, **14**, 15–21.

60 E. García-Rojas, J. Tapiador, P. Leo, C. Palomino, C. Martos and G. Orcajo, Catalytical Advantages of Hf-MOFs in Benzaldehyde Acetalization, *Catal. Today*, 2024, **434**, 114705, DOI: **10.1016/j.cattod.2024.114705**.